



Characterization of quaternary Zn/Sn-codoped GaN films obtained with $Zn_xSn_{0.04}GaN$ targets at different Zn contents by the RF reactive magnetron sputtering technology

Dong-Hau Kuo^{1,*}  and Yen-Tzu Liu¹

¹Department of Materials Science and Engineering, National Taiwan University of Science and Technology, Taipei 10607, Taiwan

Received: 2 January 2018

Accepted: 3 March 2018

Published online:
8 March 2018

© Springer Science+Business
Media, LLC, part of Springer
Nature 2018

ABSTRACT

Quaternary (Zn, Sn, Ga)N thin films with co-existing a large amount of acceptor and donor were purposely fabricated in order to heavily distort the GaN lattice and to extend the degenerated GaN semiconductor to a different aspect. The ZnSnGaN films were made of reactive sputtering with single cermet targets containing Zn, Sn, Ga, and GaN under the nitridation atmosphere. By varying the Zn content at fixed 4% Sn content, different $Zn_xSn_{0.04}Ga_{0.96-x}N$ targets at $x = 0, 0.03, 0.06,$ and 0.09 were prepared for Zn/Sn- x -GaN films. With increasing the Zn content, Zn/Sn- x -GaN due to the charge compensation changed from semiconducting n type to p type, and from high electron concentration of $4.1 \times 10^{17} \text{ cm}^{-3}$ to high hole concentration of $3.3 \times 10^{17} \text{ cm}^{-3}$. The optical band gap changed from 3.12 to 2.89 eV, related to the formation in Zn_{Ga} acceptor and Sn_{Ga} donor defects. The hetero- and homo-junction diodes were fabricated. The n - $Zn_{0.03}Sn_{0.04}GaN/p$ - $Zn_{0.09}Sn_{0.04}GaN$ homo-junction diode tested at 25 °C had the turn-on voltage of 0.9 V, leakage current density of $6.0 \times 10^{-5} \text{ A/cm}^2$ at -1 V , breakdown voltage of 4.7 V, current density of $2.4 \times 10^{-2} \text{ A/cm}^2$ at 5 V, ideality factor of 3.4, and barrier height of 0.65 eV.

Introduction

Wide-band-gap III-V nitride semiconductors such as gallium nitride (GaN) had been applied in light-emitting diodes (LEDs) and laser diodes (LD). GaN had a direct E_g of 3.4 eV and had other excellent characteristics such as thermal conductivity, high breakdown voltage, and high mobility. For LED,

epitaxial GaN layer has been deposited at 1000 °C with metal-organic Ga and ammonia as Ga and N sources, respectively.

Defect engineering to control the electrical properties of GaN has been important for the development of the p -type Mg-doped GaN in achieving the commercialization GaN-based LEDs and in winning the 2014 Nobel Prize for Physics by Prof.

Address correspondence to E-mail: dhkuo@mail.ntust.edu.tw

S. Nakamura. Alloy systems in GaN, Mg-GaN, and InGaN have been well developed due to the LED industry. There were still some efforts in doping GaN with Si, Ge, and Sn for modifying the *n*-type properties [1–3], and codoping GaN with Si donor and Zn acceptor [4–6], and with Si donor and Mg acceptor [7]. Katayama-Yoshida et al. [8] reported that the codoping method enhances the solubility of the dopant, reduces the acceptor energy level, and increases the mobility of the carriers.

The above-mentioned GaN-related films have been deposited above 800 °C by metal organic chemical vapor deposition (MOCVD) or metal–organic vapor phase epitaxy (MOVPE), which involved the high facility, operation, and maintenance costs and was difficult to be used for quaternary system due to the need of ~ 6 gas-flow lines. In recent years, we have developed the reactive sputtering technology with cermet targets for *n*- or *p*-type GaN-based semiconducting thin films and diodes with material systems of GaN, InGaN, AlInGaN, Mg-GaN, Mg-InGaN, Zn-GaN, and Sn-GaN [9–14]. The drawback of our works is to have films in a polycrystalline nature. However, it has its merits in diversity, flexibility, cost effectiveness, etc. Multicomponent and extremely complex GaN-based semiconductor thin films can be easily deposited with our technology to change its photosensitivity into the visible-light range. Giving an example, (Ga, Zn)(O, N) has been viewed as a potential visible-light photocatalyst for the water splitting [15, 16].

In this work, we fabricated Zn/Sn-codoped GaN thin films on Si (100) wafers by the technique of RF reactive sputtering with $Zn_xSn_{0.04}Ga_{0.96-x}N$ single cermet targets at fixed 4% Sn and different Zn contents at $x = 0, 0.03, 0.06, \text{ and } 0.09$ for the purposes of understanding the codoping solubility, process ability, process window, and performance. Conventionally, GaN is a wide-band-gap semiconductor and acts as a UV light photosensitizer or a LED component. To extend its applications for photocatalysis, it needs the high free energy by increasing entropy with solid solutioning and the *p*-type form in order to fabricate the nanodiodes for enhancing the charge separation [17]. By establishing and identifying the database of this materials system under different doping conditions, the semiconducting visible-light photosensitizer and photocatalyst can be designed and fulfilled.

Experimental procedure

Zn/Sn-codoped GaN or Zn/Sn-*x*-GaN thin films on Si (100) substrates were prepared by radio-frequency (RF) reactive sputtering with single (Zn + Sn + Ga + GaN) cermet targets containing 0, 3, 6, or 9 mol% Zn and 4 mol% Sn in an Ar/N₂ atmosphere. Zn/Sn-*x*-GaN films prepared with the targets at different Zn contents are abbreviated as Zn/Sn-*x*-GaN with $x = 0, 0.03, 0.06, \text{ and } 0.09$. The cermet target was fabricated by hot pressing the powder mixture of Ga, Zn, Sn, and GaN in according to the composition design at $(Ga_{0.9}Zn_{0.06}Sn_{0.04})N$. During the deposition, the chamber pressure was pumped down to 1×10^{-6} torr by diffusion pump before sputtering, while 9×10^{-3} torr during sputtering. The gas mixture had an Ar flow rate of 5 sccm and the N₂ flow rate of 10 sccm.

X-ray diffractometry (XRD, D8 Discover, Bruker) and high-resolution transmission electron microscopy (HR-TEM, Tecnai G2, Philips) have been used to study the crystal structure of Zn/Sn-*x*-GaN films. Scanning electron microscopy (SEM, JSM-6500F, JEOL) and atomic force microscopy (AFM, Dimension Icon, Bruker) were employed to analyze the surface morphology and topography of Zn/Sn-*x*-GaN films. Compositional analyses of these films were conducted by the energy-dispersive spectrometer (EDS, JSM-6500F, JEOL) provided on SEM. The element mapping of catalysts was performed by scanning transmission electron microscopy (STEM, Tecnai G2 F20, Philips). A Hall measurement system (HMS-2000, Ecopia) with a maximum magnetic field of 0.51 T was used to measure electrical properties. Ultraviolet–visible (UV–Vis) spectrometer (V-670, Jasco) was used for the absorption spectra.

Results and discussion

EDS composition analyses of the Zn/Sn-*x*-GaN films prepared at 400 °C with Zn_xSnGaN targets at $x = 0, 0.03, 0.06, \text{ and } 0.09$ are shown in Table 1. Under the deposition conditions of 120 W and 400 °C, all films deposited with different $Zn_xSn_{0.04}GaN$ targets showed the close Sn content of 0.045 ± 0.023 in average. With the Zn increase in target, the Zn/Sn-*x*-GaN film had a higher Zn content and a lower Ga content. The $[Zn]/([Ga] + [Zn] + [Sn])$ ratios were 0, 0.045, 0.066, and 0.086 and the $[Ga]/([Ga] + [Zn] +$

Table 1 Compositional analyses of Zn/Sn-*x*-GaN films deposited at 400 °C with Zn_{*x*}SnGaN targets at (a) *x* = 0, (b) *x* = 0.03, (c) *x* = 0.06, and (d) *x* = 0.09

<i>x</i> in Zn _{<i>x</i>} SnGaN	Ga (at.%)	Zn (at.%)	Sn (at.%)	N (at.%)	[Zn]/[Ga + Sn + Zn]	[Sn]/[Ga + Sn + Zn]	[N]/[Ga + Sn + Zn]
0	49.02	–	2.19	48.78	–	0.043	0.953
0.03	46.78	2.34	2.54	48.34	0.045	0.049	0.936
0.06	46.69	3.47	2.48	47.36	0.066	0.047	0.900
0.09	45.46	4.52	2.16	47.85	0.086	0.042	0.918

[Sn]) ratios were 0.957, 0.906, 0.887, and 0.872. The film compositions were quite close to the design formula at (Ga_{0.96-*x*}Zn_{*x*}Sn_{0.04})N. The N content at the average [N]/([Ga] + [Zn] + [Sn]) ratio of 0.927 ± 0.023 was slightly deficient. The Zn/Sn-*x*-GaN films contained the few donor defects in nitrogen vacancy.

Figure 1 shows XRD patterns of the Zn/Sn-*x*-GaN films deposited at 400 °C with Zn_{*x*}SnGaN targets at (a) *x* = 0, (b) *x* = 0.03, (c) *x* = 0.06, and (d) *x* = 0.09. XRD results indicated that all Zn/Sn-*x*-GaN films grown on Si (100) substrates were polycrystalline and had a wurtzite structure with a preferential growth orientation from the (10 $\bar{1}$ 0) plane. The other weak diffraction peaks were contributed from the (0002), (10 $\bar{1}$ 1), (11 $\bar{2}$ 0), (20 $\bar{2}$ 0), (11 $\bar{2}$ 2), and (20 $\bar{2}$ 1) planes, all indicated in Fig. 1 with different symbols. There were no other second phases detected. Lattice constant of *a* was not changed with the Zn addition in Zn/Sn-*x*-GaN films, but *c* and the unit-cell volume of Zn/Sn-*x*-GaN films slightly increased. The *c* values were 5.17, 5.19, 5.20, and 5.23 Å and the values of unit-cell volume were 45.67, 46.28, 46.52, and 46.88 Å³ for Zn/

Sn-*x*-GaN films at *x* = 0, 0.03, 0.06, and 0.09, respectively. As Zn of 0.88 Å and Sn of 0.83 Å have the larger ionic sizes than Ga of 0.76 Å, the substitution of Ga with Zn and Sn is expected to expand the unit cell. The full-width-half-maximum (FWHM) values of the (10 $\bar{1}$ 0) peak in terms of the 2θ value increased with the Zn incorporation, and they were 0.34°, 0.43°, 0.46°, and 0.59°. The FWHM values increased with the Zn incorporation, indicating the Zn addition degraded the film crystallinity. Based upon the Scherrer’s equation of $D = K\lambda/\beta \cos \theta$, where *D* is the crystallite size, *K* a constant of 0.9, λ the X-ray wavelength, (β) the line broadening at FWHM, and (θ) the diffraction angle, the crystallite sizes were 24.3, 19.2, 17.9, and 14.0 nm. Table 2 lists all the derived data from the XRD measurement.

Figure 2 shows SEM surface images of Zn/Sn-*x*-GaN films deposited at 400 °C with Zn_{*x*}SnGaN targets at (a) *x* = 0, (b) *x* = 0.03, (c) *x* = 0.06, and (d) *x* = 0.09. Zn/Sn-*x*-GaN films were dense and had a good contact with the Si substrate. The film/substrate interface did not show cracks. From the insets in each image, Zn/Sn-*x*-GaN films had the close thickness of ~ 1.0 μm or ~ 33 nm/min in growth rate. The film growth rate did not change with the Zn content in target. From the cross-sectional images, there were no characteristic cracking traces. The images also reveal the grain size reduction with the increase at the Zn content in Zn/Sn-*x*-GaN films, which is consistent with the data derived from the Scherrer’s equation.

The AFM morphologies of Zn/Sn-GaN films after scanning on the 5 × 5 μm² dimension are shown in Fig. 3. The root-mean-square (Rms) roughness values of Zn/Sn-*x*-GaN films decreased from 3.39, 3.06, 2.90 to 1.43 nm as films deposited with Zn_{*x*}SnGaN targets increased its Zn content from *x* = 0, 0.03, 0.06 to 0.09. The Zn addition apparently improved the surface roughness of the Zn/Sn-*x*-GaN films. As the films

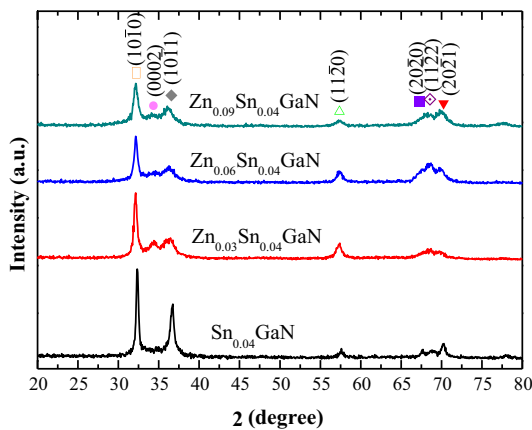
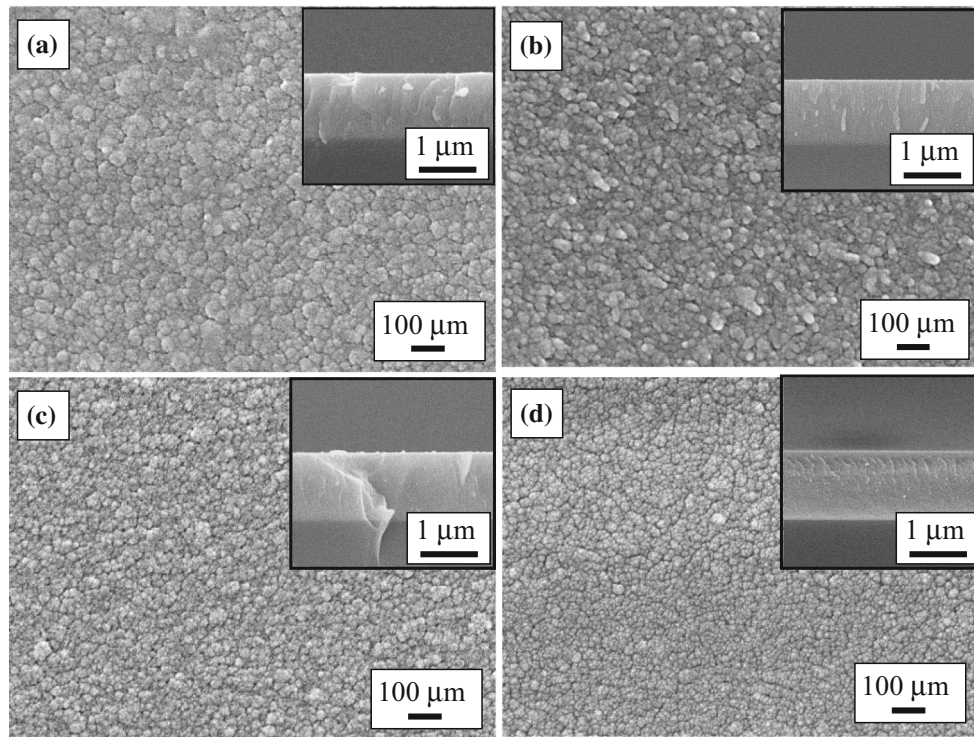


Figure 1 XRD patterns of Zn/Sn-*x*-GaN films deposited at 400 °C with Zn_{*x*}SnGaN targets at **a** *x* = 0, **b** *x* = 0.03, **c** *x* = 0.06, and **d** *x* = 0.09.

Table 2 Structure properties of Zn/Sn- x -GaN films deposited at 400 °C with Zn $_x$ SnGaN targets at (a) $x = 0$, (b) $x = 0.03$, (c) $x = 0.06$, and (d) $x = 0.09$

x in Zn $_x$ SnGaN	Deposition temp./°C	2θ (10 $\bar{1}0$) peak	a (Å)	c (Å)	Volume (Å ³)	FWHM (10 $\bar{1}0$) (°)
0	100	32.35	3.19	5.17	45.67	0.34
0.03	200	32.20	3.20	5.19	46.28	0.43
0.06	300	32.15	3.21	5.20	46.52	0.46
0.09	400	32.15	3.21	5.23	46.88	0.59

**Figure 2** SEM surface images of Zn/Sn- x -GaN films deposited at 400 °C with Zn $_x$ SnGaN targets at **a** $x = 0$, **b** $x = 0.03$, **c** $x = 0.06$, and **d** $x = 0.09$.

from targets of different Zn contents had the close growth rates, the great improvement in surface roughness was not caused by the change in growth rate but the Zn dopant effect on growth kinetics to make the grains finer due to the enhanced solid solutioning to retard the grain growth. The finer grains have its behavior toward the glassy phase with nanodomains, which lead to the smoother film surface.

Electrical properties of Zn/Sn- x -GaN films were measured by Hall measurement system at room temperature. Figure 4 shows the variations of electrical properties of (a) carrier concentration, (b) mobility, and (c) electrical conductivity of Zn/Sn- x -GaN films deposited at 400 °C with Zn $_x$ SnGaN targets at

$x = 0, 0.03, 0.06$, and 0.09 . The Zn/Sn- x -GaN films presented as an n -type semiconductor at $x = 0$ and 0.03 but a p -type one at $x = 0.06$ and 0.09 . The carrier concentrations (n_e) were 4.1×10^{17} and $7.5 \times 10^{16} \text{ cm}^{-3}$ for Zn/Sn- x -GaN at $x = 0$ and 0.03 , respectively, while the n_p values were 1.8×10^{16} and $3.3 \times 10^{17} \text{ cm}^{-3}$ at $x = 0.06$ and 0.09 . The electron mobilities (μ) were 8.5 and $11 \text{ cm}^2/\text{V s}$ for Zn/Sn- x -GaN at $x = 0$ and 0.03 , respectively, while they were 23 and $3 \text{ cm}^2/\text{V s}$ at $x = 0.06$ and 0.09 , respectively. The electron conductivities (σ) were 0.55 and 0.15 S cm^{-1} for Zn/Sn- x -GaN at $x = 0$ and 0.03 , respectively, while they were 0.06 and 0.16 S cm^{-1} at $x = 0.06$ and 0.09 , respectively. Zn/Sn-0-GaN film or the Sn-doped GaN was an n -type semiconductor with

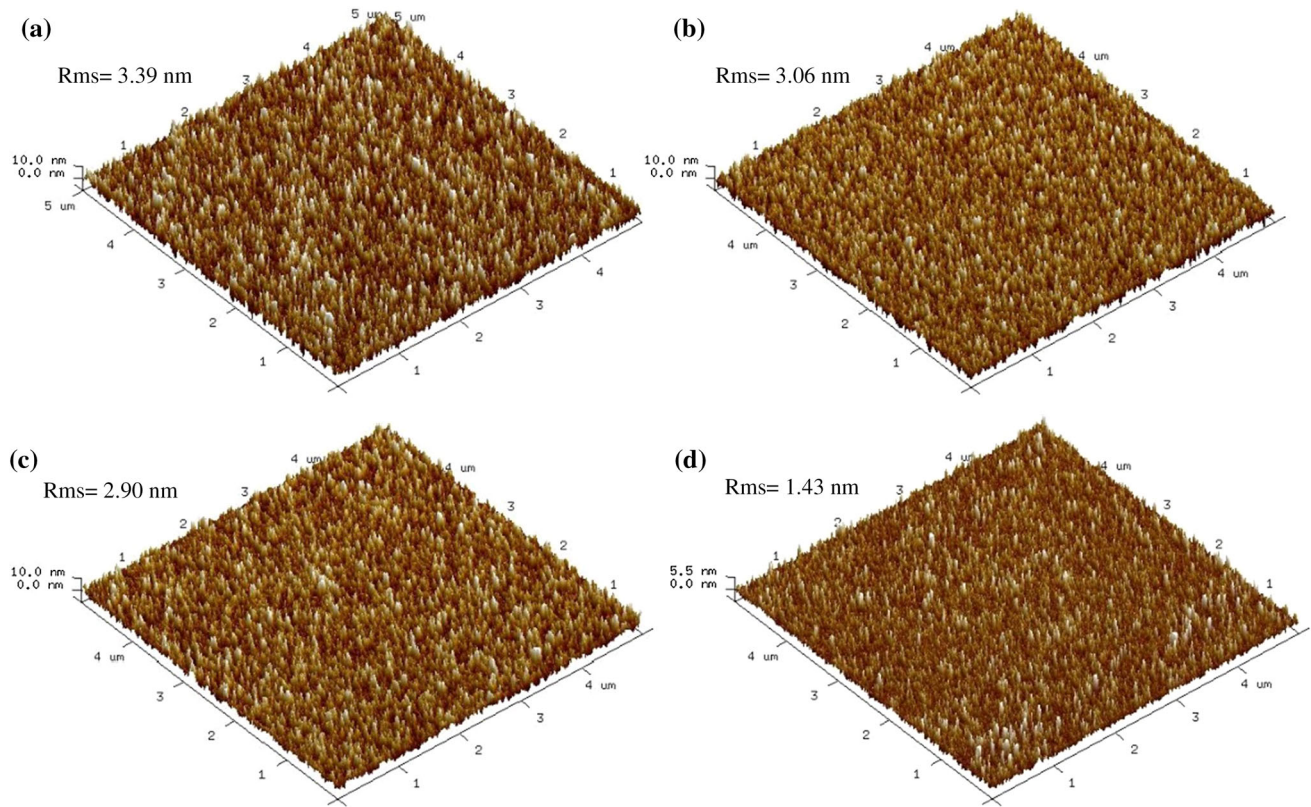


Figure 3 3D-AFM morphologies of Zn/Sn- x -GaN films deposited at 400 °C with Zn $_x$ SnGaN targets at **a** $x = 0$, **b** $x = 0.03$, **c** $x = 0.06$, and **d** $x = 0.09$.

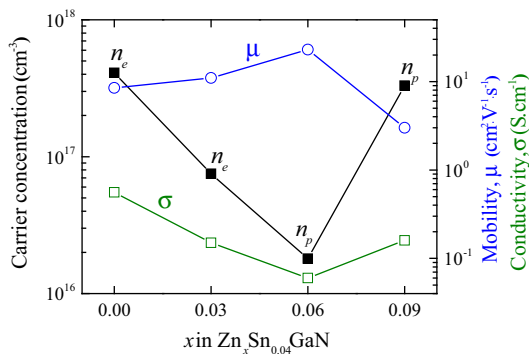


Figure 4 Variations of electrical properties of carrier concentration, mobility, and electrical conductivity of Zn/Sn- x -GaN films deposited at 400 °C with Zn $_x$ SnGaN targets at $x = 0, 0.03, 0.06$, and 0.09 .

a high carrier concentration of $4.1 \times 10^{17} \text{ cm}^{-3}$. The addition of Zn acceptor with the increased concentration into SnGaN can compensate electrons from Sn donor with holes from Zn acceptor. Therefore, the electron concentration drops with the increase at the Zn content. Once the hole concentration from Zn acceptor dominates over the electron concentration, a

minimum in carrier concentration reached for the p -type Zn/Sn-0.06-GaN film. If the Zn content further increases, the hole concentration increases and p -type Zn/Sn-0.09-GaN has the improved electrical properties. The benefit for the design of the transition from the n -type to the p -type transition is to show the controllability of the heavily doped GaN in the semiconductor properties at a wide range.

UV-Vis spectrometer was used to measure the coefficient of absorption for the optical band gap (E_g) values of Zn/Sn- x -GaN films. From the UV-Vis spectrum results, the absorption coefficient and E_g of films could be figured by Tauc equation, which is presented as equation: $(\alpha h\nu)^2 = A (h\nu - E_g)$, where α is optical absorption coefficient, A a constant, $h\nu$ the incident photon energy, and E_g the energy band gap of the Zn/Sn- x -GaN films. From plotting the $(\alpha h\nu)^2 - h\nu$ curves, the optical band gap of Zn/Sn- x -GaN films could be directly obtained by extrapolating the linear part of the curves, as shown in Fig. 5a. The extrapolated E_g values were 3.12, 3.07, 3.0, and 2.89 eV for Zn/Sn- x -GaN films deposited at 400 °C with Zn $_x$ -SnGaN targets at $x = 0, 0.03, 0.06$, and 0.09 ,

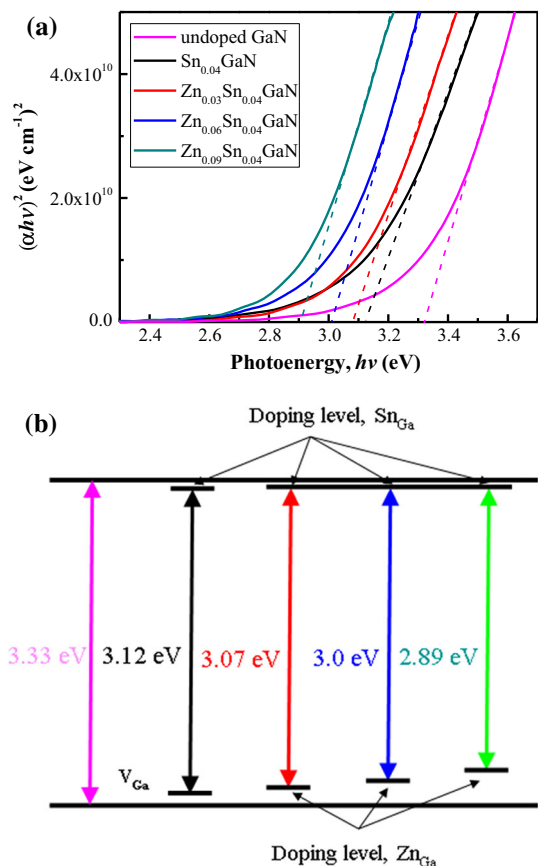


Figure 5 a Plots of $(\alpha hv)^2$ versus photon energy ($h\nu$) for the optical band gap determination of Zn/Sn- x -GaN films deposited at 400 °C with Zn $_x$ SnGaN targets at $x = 0, 0.03, 0.06,$ and 0.09 . b The proposed band diagram for the Zn/Sn-co-doped GaN films.

respectively, while the pure GaN has an E_g value of 3.33 eV. The 4% Sn incorporation had E_g changed from 3.33 to 3.12 eV due to the formed Sn_{Ga} donor defect. The Zn addition from 0 to 9% further decreased E_g from 3.12 to 2.89 eV due to the form Zn_{Ga} acceptor. Sn had formed the shallow Sn_{Ga} donor level located 33 meV below conduction band [3], while Zn formed the deeper Zn_{Ga} acceptor level located 200–400 meV above the valance band [18–20]. Here, our E_g values also became smaller with the increase in the Zn content (Fig. 5a). The deep V_{Ga} (Ga vacancy) acceptor defect was identified in the n -type Si-doped [21] and Zn/Si-codoped GaN [6]. With the addition of the Zn acceptor substituent, the V_{Ga} defect was replaced by Zn_{Ga} acceptor defect. With the addition of Sn donor, the shallow V_{N} (nitrogen vacancy) donor defect was replaced. Therefore, the variation of the band gap with the Zn and Sn defect concentration is shown in Fig. 5b.

To confirm the semiconductor type, the hetero-junction diodes were fabricated. Figure 6 shows electrical properties of (a) n -(Zn/Sn- x -GaN)/ p -Si and (b) p -(Zn/Sn- x -GaN)/ n -Si hetero-junction diodes tested at room temperature on a square contact of 1 mm². The applied voltage had a range of $-10 \sim +10$ V. All the diodes showed the rectifying behaviors without breakdown. For the n -Zn/Sn- x -GaN diodes at $x = 0$ and 0.03 , the leakage current densities of the diodes were found to be 1×10^{-4} and 2×10^{-4} A/cm² under the reverse bias of -1 V, turn-on voltages of 1.5 and 1.7 V, the forward current densities of 4.11×10^{-1} and 7.64×10^{-2} A/cm² under the bias of 10 V, respectively. The diode with the higher σ value of n -Zn/Sn-0-GaN showed the higher forward current density than that made with Zn/Sn-0.03-GaN. For the p -Zn/Sn- x -GaN diodes at $x = 0.06$ and 0.09 , the leakage current densities of the diodes were found to be 2.2×10^{-4} and 3×10^{-4} A/cm² under the reverse bias of -1 V, turn-on voltages of 1.8 and 2.0 V, the forward current densities of 6.9×10^{-2} and 1.5×10^{-1} A/cm² under the bias of 10 V, respectively. The diode with the higher σ value of p -Zn/Sn-0.09-GaN showed the higher forward current density than that made with Zn/Sn-0.06-GaN. Based upon the thermionic-emission theory and semiconductor properties from I - V test [22], the hetero-junction diodes had the ideality factors of 6.5, 6.4, 6.3, and 6.1 and barrier heights of 0.59, 0.64, 0.63, and 0.64 eV for devices made with Zn/Sn- x -GaN at $x = 0, 0.03, 0.06,$ and 0.09 , respectively. The heavily acceptor/donor-codoped GaN semiconductor can be the reason for the much higher ideality factor.

n -Zn_{0.03}Sn_{0.04}GaN and p -Zn_{0.09}Sn_{0.04}GaN were used to demonstrate the heavily doped GaN in making a special type of homo-junction diode. Figure 7 shows the forward and reverse current–voltage (I - V) characteristics of n -Zn_{0.03}Sn_{0.04}GaN/ p -Zn_{0.09}Sn_{0.04}GaN homo-junction diode tested in the temperature range of 25–150 °C. This homo-junction diode tested at 25 °C had turn-on voltage of 0.9 V, leakage current density of 6.0×10^{-5} A/cm² at -1 V, breakdown voltage of 4.7 V, current density of 2.4×10^{-2} A/cm² at 5 V, ideality factor of 3.4, and barrier height of 0.65 eV. With the test temperature increasing to 150 °C, leakage current density increased to 5.9×10^{-4} A/cm², ideality factor dropped to 2.6, and barrier height increased to 0.92 eV. The I - V measurement identifies the rectifying

Figure 6 Electrical properties of **a** n -(Zn/Sn- x -GaN)/ p -Si and **b** p -(Zn/Sn- x -GaN)/ n -Si hetero-junction diodes measured at room temperature.

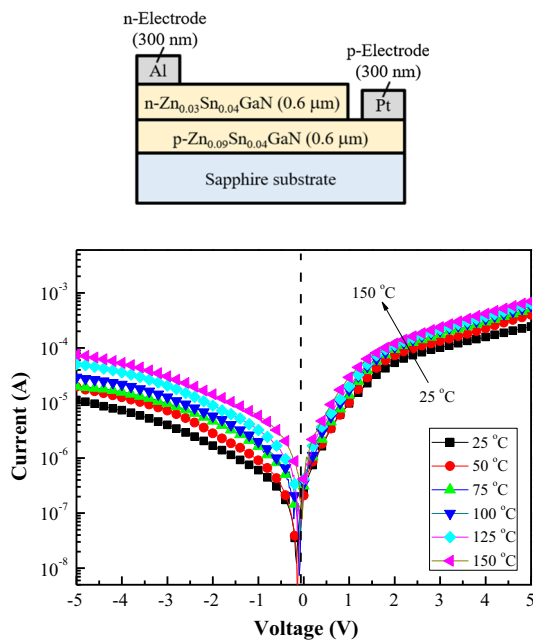
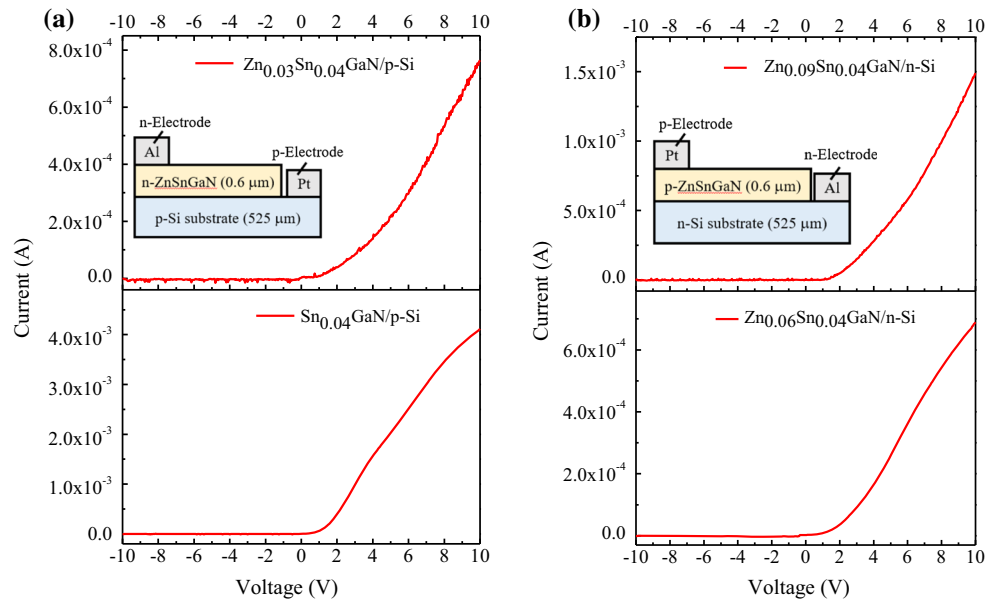


Figure 7 The forward and reverse current–voltage (I – V) characteristics of n -Zn_{0.03}Sn_{0.04}GaN/ p -Zn_{0.09}Sn_{0.04}GaN homo-junction diode tested in the temperature range of 25–150 °C.

behavior of n -GaN/ p -GaN diode made of the heavily doped Zn acceptor and Sn donor.

Conclusions

Zn acceptor was incorporated into the n -type 4% Sn-doped GaN to form the acceptor/donor-codoped Zn/Sn- x -GaN thin films made of RF magnetron reactive sputtering with single cermet Zn _{x} Sn_{0.04}GaN targets at $x = 0, 0.03, 0.06,$ and 0.09 . With increasing the Zn amount in target, the tertiary Sn_{0.04}GaN films became quaternary Zn/Sn-GaN film with the same wurtzite structure, the n -to- p transition, and the slightly increased lattice constant of the c axis and the unit-cell volume. The codoping extended the electrical properties to a wide range from n_e of $4.0 \times 10^{17} \text{ cm}^{-3}$ to n_p of $3.3 \times 10^{17} \text{ cm}^{-3}$. The codoping is an approach to fabricate the degenerated semiconductor with the highly compensated acceptor and donor. The acceptor/donor-codoped semiconductor and its device were filled with defects to narrow their optical band gap from 3.12 for SnGaN to 2.89 eV for visible-light-excitable ZnSnGaN. Hetero-junction Zn/Sn-GaN diodes had the poor rectifying behavior but had a low leakage current and did not breakdown at the range of $-10 \sim +10$ V. The homo-junction Zn/Sn-GaN diode showed the improved rectifying behavior with stability up to 150 °C and low leakage current density of $6.0 \times 10^{-5} \text{ A/cm}^2$ at -1 V but had a lower breakdown voltage of 4.7 V.

Acknowledgements

This work was supported by the Ministry of Science and Technology of the Republic of China under Grant Number MOST 104-2221-E-011-169-MY3.

References

- [1] Shuji N, Takashi M, Masayuki S (1992) Si- and Ge-doped GaN films grown with GaN buffer layers. *Jpn J Appl Phys* 31:2883–2888
- [2] Molina SI, Sánchez AM, Pacheco FJ, Garcia R, Sánchez-Garcia MA, Sánchez FJ, Calleja E (1999) The effect of Si doping on the defect structure of GaN/AlN/Si(111). *Appl Phys Lett* 74:3362–3364
- [3] Shikanaia A, Fukahori H, Kawakami Y, Hazu K, Sota T, Mitani T, Mukai T, Fujita S (2003) Optical properties of Si-, Ge- and Sn-doped GaN. *Phys Status Solidi (b)* 235:26–30
- [4] Nakamura S, Mukai T, Senoh M (1994) Candela-class high-brightness InGaN/AlGaIn double-heterostructure blue-light-emitting diodes. *Appl Phys Lett* 64:1687–1689
- [5] Sheu JK, Pan CJ, Chi GC, Kuo CH, Wu LW, Chen CH, Chang SJ, Su JK (2002) White-light emission from InGaN–GaIn multiquantum-well light-emitting diodes with Si and Zn codoped active well layer. *IEEE Photo Technol Lett* 14:450–452
- [6] Reshchikov MA, Foussekis M, McNamara JD, Behrends A, Bakin A, Waag A (2012) Determination of the absolute internal quantum efficiency of photoluminescence in GaN co-doped with Si and Zn. *J Appl Phys* 111:073106
- [7] Kim KS, Yang GM, Lee HJ (1999) The study on the growth and properties of Mg doped and Mg-Si codoped p-type GaN. *Solid State Electron* 43:1807–1812
- [8] Katayama-Yoshida H, Kato R, Yamamoto T (2001) New valence control and spin control method in GaN and AlN by codoping and transition atom doping. *J Cryst Growth* 231:428–436
- [9] Ting CW, Thao CP, Kuo DH (2017) Electrical and structural characteristics of tin-doped GaN thin films and its hetero-junction diode made all by RF reactive sputtering. *Mater Sci Semicond Proc* 59:50–55
- [10] Li CC, Kuo DH (2014) Effects of growth temperature on electrical and structural properties of sputtered GaN films with a cermet target. *J Mater Sci Mater Electron* 25:1404–1409
- [11] Tuan TTA, Kuo DH, Chen CC, Yen WC (2014) Schottky barrier characteristics of Pt contacts to all sputtering-made n-type GaN and MOS diodes. *J Mater Sci Mater Electron* 25:3264–3270
- [12] Kuo DH, Tran TTA, Chen CC, Yen WC (2015) Electrical and structural properties of Mg-doped $\text{In}_x\text{Ga}_{1-x}\text{N}$ ($x \leq 0.1$) and p-InGaIn/n-GaN junction diode made all by RF reactive sputtering. *Mater Sci Eng B* 193:13–19
- [13] Kuo DH, Li CC, Tran TTA, Yen WC (2015) Effects of Mg doping on the performance of InGaIn films made by reactive sputtering. *J Electron Mater* 44:210–216
- [14] Lin K, Kuo DH (2017) Characteristics and electrical properties of reactively sputtered AlInGaIn films from three different $\text{Al}_{0.05}\text{In}_x\text{Ga}_{0.95-x}\text{N}$ targets with $x = 0.075, 0.15,$ and 0.25 . *Mater Sci Semicond Proc* 57:63–69
- [15] Maeda K, Teramura K, Saito N, Inoue Y, Kobayashi H, Domen K (2006) Overall water splitting using (oxy)nitride photocatalysts. *Pure Appl Chem* 78:2267–2276
- [16] Maeda K, Teramura K, Domen K (2008) Effect of post-calcination on photocatalytic activity of $(\text{Ga}_{1-x}\text{Zn}_x)(\text{N}_{1-x}\text{O}_x)$ solid solution for overall water splitting under visible light. *J Catal* 254:198–204
- [17] Abdullah H, Kuo DH (2015) Photocatalytic performance of Ag and CuBiS_2 nanoparticles-coated $\text{SiO}_2@\text{TiO}_2$ composite sphere under visible and ultraviolet light irradiation for azo dye degradation with the assistance of numerous nano p-n diodes. *J Phys Chem C* 119:13632–13641
- [18] Neugebauer J, Van de Walle CG (1999) Chemical trends for acceptor impurities in GaN. *J Appl Phys* 85:3003–3005
- [19] Lyons JL, Janotti A, Van de Walle CG (2013) Impact of group-II acceptors on the electrical and optical properties of GaN. *Jpn J Appl Phys* 52:08JJ04
- [20] Demchenko DO, Reshchikov MA (2013) Blue luminescence and Zn acceptor in GaN. *Phys Rev B* 88:115204
- [21] Li D, Ma B, Miyagawa R, Hu W, Narukawa M, Miyake H, Hiramatsu K (2009) Photoluminescence study of Si-doped a-plane GaN grown by MOVPE. *J Cryst Growth* 311:2906–2909
- [22] Tuan TTA, Kuo DH, Saragih AD, Li GZ (2017) Electrical properties of RF-sputtered Zn-doped GaN films and p-Zn-GaN/n-Si hetero junction diode with low leakage current of 10^{-9} A and a high rectification ratio above 10^5 . *Mater Sci Eng B* 222:18–25